SUPPLEMENTAL MATERIAL

$Ca_V3.2$ Channels and the Induction of Negative Feedback in Cerebral Arteries

Osama F. Harraz[1,2,*], Rasha R. Abd El-Rahman[1,*], Kamran Bigdely-Shamloo[1,3], Sean M. Wilson[4], Suzanne E. Brett[1], Monica Romero[4], Albert L. Gonzales[5], Scott Earley[6], Edward J. Vigmond[3,7], Anders Nygren[3], Bijoy K. Menon[8], Rania E. Mufti[1], Tim Watson[8], Yves Starreveld[8], Tobias Furstenhaupt[9], Philip R. Muellerleile[10], David Kurjiaka[10], Barry D. Kyle[1], Andrew P. Braun[1] and Donald G. Welsh[1,#]

* OFH and RRA are co-first authors and contributed equally to the manuscript

[1] Dept. of Physiology and Pharmacology, Hotchkiss Brain and Libin Cardiovascular Institutes, University of Calgary, Calgary, AB, Canada
[2] Dept. of Pharmacology and Toxicology, Alexandria University, Alexandria, Egypt
[3] Dept. of Electrical and Computer Engineering, University of Calgary, Calgary, AB, Canada
[4] Division of Pharmacology, Loma Linda University, Loma Linda, CA, USA
[5] Dept. of Biomedical Sciences, Colorado State University, Fort Collins, CO, USA
[6] Dept. of Pharmacology, University of Nevada, Reno, NV, USA
[7] LIRYC Institute and Lab IMB, University of Bordeaux, Bordeaux, France
[8] Dept. of Clinical Neurosciences, University of Calgary, Calgary, AB, Canada
[9] Microscopy Imaging Facility, University of Calgary, Calgary, AB, Canada
[10] Dept. of Biomedical Sciences, Grand Valley State University, Allendale, MI, USA

Running Title: Vascular $Ca_V3.2$ and Negative Feedback

[#] Corresponding Author: Donald G. Welsh, PhD (dwelsh@ucalgary.ca)

SUPPLEMENTAL MATERIALS AND METHODS

Animal Procedures

Animal procedures were approved by the Animal Care and Use Committee at the University of Calgary. Briefly, female Sprague–Dawley rats (10–12 weeks of age) were killed via CO_2 asphyxiation. The brain was carefully removed and placed in cold phosphate-buffered saline (PBS, pH 7.4) solution containing (in mM): 138 NaCl, 3 KCl, 10 Na_2HPO_4, 2 NaH_2PO_4, 5 glucose, 0.1 $CaCl_2$ and 0.1 $MgSO_4$. Middle and posterior cerebral arteries were carefully dissected out of surrounding tissue and cut into 2–3 mm segments. Human brain samples, from which small cerebral arteries (150 to 250 µm-diameter), were obtained with institutional review board approval and written informed consent according to the *Declaration of Helsinki*.

Isolation of Cerebral Arterial Smooth Muscle Cells

Smooth muscle cells from middle and posterior cerebral arteries were enzymatically isolated as previously described. Briefly, arterial segments were placed in an isolation medium (37 °C, 10 min) containing (in mM): 60 NaCl, 80 Na-glutamate, 5 KCl, 2 $MgCl_2$, 10 glucose and 10 HEPES with 1 mg/ml bovine serum albumin (pH 7.4). Vessels were then exposed to a two-step digestion process that involved: 1) 12-15 min incubation in isolation medium (37 °C) containing 0.5 mg/ml papain and 1.5 mg/ml dithioerythritol; and 2) a 15 minutes incubation in isolation medium containing 100 µM Ca^{2+}, 0.7 mg/ml type F collagenase and 0.4 mg/ml type H collagenase. Following incubation, tissues were washed repeatedly with ice-cold isolation medium and triturated with a fire-polished pipette. Liberated cells were stored in ice-cold isolation medium for use the same day within ~5 hr.

Electrophysiological Recordings

Conventional patch-clamp electrophysiology was used to monitor whole-cell voltage-gated Ca^{2+} channel currents in isolated smooth muscle cells as reported earlier. Recording electrodes (5-8 MΩ) were pulled from borosilicate glass microcapillary tubes (Sutter Instruments, Novato, CA) using a micropipette puller (Narishige PP-830, Tokyo, Japan), and backfilled with pipette solution (in mM): 135 CsCl, 5 Mg-ATP, 10 HEPES, and 10 EGTA (pH 7.2). Cells were voltage-clamped and equilibrated in bath solution (in mM): 110 NaCl, 1 CsCl, 10 $BaCl_2$, 1.2 $MgCl_2$, 10 glucose, and 10 HEPES (pH 7.4). A NaCl-agar bridge was used between the reference electrode and the bath solution. To record whole-cell currents, isolated cells held at -60 mV were exposed to a pre-pulse (-90 mV, 200 ms) and then voltage steps ranging from -50 to +40 mV (10 mV interval, 300 ms).

Perforated patch-clamp electrophysiology was used to measure whole-cell K^+ currents in isolated smooth muscle cells. The bath solution contained (in mM): 134 NaCl, 4 KCl, 2 $MgCl_2$, 2 $CaCl_2$, 10 glucose, and 10 HEPES (pH 7.4). The pipette solution contained (in mM): 110 K aspartate, 30 KCl, 10 NaCl, 2 $MgCl_2$, 10 HEPES, and 0.05 EGTA (pH 7.2) with 200 µg/ml amphotericin B. Membrane currents were recorded while the cells were: 1) held at a steady membrane potential of -40 and -20 mV; or 2) slowly ramped from -60 to +20 mV (4mV/s). Whole-cell currents were recorded using an Axopatch 200B patch-clamp amplifier (Molecular Devices, Sunnyvale, CA), filtered at 1 kHz, digitized at 5 kHz, and were stored on a computer for offline analysis with Clampfit 10.3 software (Molecular Devices, Sunnyvale, CA). Whole-cell capacitance averaged 14-18 pF and was measured with the cancellation circuitry in the voltage-clamp amplifier. A 1 M NaCl–agar salt bridge between the reference electrode and the bath

solution was used to minimize offset potentials (<2 mV). All electrophysiological experiments were performed at room temperature (~22ºC). STOC analysis was performed with customized software provided by B. Hald (University of Copenhagen); threshold for detection was set at 3 times the BK_{Ca} single channel conductance.

In a small complement of experiments, single channel currents were monitored using the on-cell configuration. The bath solution contained: 145 mM KCl, 1 mM $CaCl_2$, 10 mM HEPES, and 200 nM nifedipine (pH 7.4). The pipette solution contained: 60 mM $CaCl_2$, 50 mM TEA-Cl, 10 mM HEPES, and 200 nM nifedipine (pH 7.2). Single channel currents were filtered at 2 kHz, digitized at 5 kHz, and stored on a computer for offline analysis with Clampfit 10.3 software (Molecular Devices, Sunnyvale, CA). Cellular patches were voltage-clamped at a holding V_M of -60 mV. To elicit single channel currents, a pre-pulse (-90 mV, 250 ms) was followed by test pulses (300 ms, -60 to -10 mV; 10 mV intervals). Recordings were performed at 22 °C. Slope conductance was calculated as described previously (Fox AP, Nowycky MC, Tsien RW (1987) Single-channel recordings of three types of calcium channels in chick sensory neurons.J Physiol 394:173-200).

Vessel Myography and Membrane Potential Measurement

Arterial segments were mounted in a customized arteriograph and superfused with warm (37 °C) physiological salt solution (PSS; pH 7.4; 21% O_2, 5% CO_2, balance N_2) containing (in mM): 119 NaCl, 4.7 KCl, 20 $NaHCO_3$, 1.1 KH_2PO_4, 1.2 $MgSO_4$, 1.6 $CaCl_2$ and 10 glucose. To limit the endothelial influence on myogenic tone development, air bubbles were passed through the vessel lumen (1–2 min); successful removal of the endothelium was confirmed by the loss of bradykinin-induced dilation. Arteries were equilibrated at 15 mmHg and the contractile responsiveness was assessed by brief application of 60 mM KCl. Following equilibration, intravascular pressure was incrementally elevated from 20 to 100 mmHg and arterial external diameter was monitored under control conditions and in the presence of paxilline (1 μM, BK_{Ca} inhibitor) and/or Ni^{2+} (50 μM, $Ca_V3.2$ blocker). Maximal arterial diameter was subsequently assessed in Ca^{2+}-free PSS (zero externally added Ca^{2+} + 2 mM EGTA). Smooth muscle membrane potential (V_M) was assessed by inserting a glass microelectrode backfilled with 1 M KCl (tip resistance = 120–150 MΩ) into the vessel wall. Measurements of V_M were first made at 60 mmHg and then in the presence of Ni^{2+} (50 μM). The criteria for successful cell impalement included: 1) a sharp negative V_M deflection upon insertion; 2) a stable recording for at least 1 min following entry; and 3) a sharp return to baseline upon electrode removal.

Electron Tomography

Whole animals were fixed similarly to immunohistochemical analysis. Brains were then removed and post-fixed in 4% paraformaldehyde (22 °C, 1 h) and cerebral arteries were isolated. Arteries were immersed in 1.6% paraformaldehyde and 2.5% glutaraldehyde in 0.1 M cacodylate buffer at pH 7.4 at 4 °C overnight. After washing three times with the same previous buffer, the samples were post-fixed in 1% osmium tetroxide buffered with cacodylate for 1 h at 22 °C, dehydrated through a graded series of acetone concentration (30–100%) and embedded in Epon 812 mixture resin. Thick sections (300-400 nm) were cut on a Reichert-Jung Ultracut E microtome using a diamond knife and collected on single hole grids with Formvar supporting film. The sections were first stained with 20% aqueous uranyl acetate/Reynolds's lead citrate and then placed on one side of a transmission electron microscopy slot grid (1×2 mm slot) covered with a continuous formvar film (~40 nm) to dry (10 min). Colloidal gold particles (10 nm

diameter) were then placed on both sides of the grid to serve as fiducial markers, and a thin carbon coating was applied for mechanical stabilization and to reduce electric charging. Once prepared, sections were viewed on a Tecnai F20 transmission electron microscope (200 keV), regions of interest were defined, and images were captured on a 1,024 × 1,024 charge-coupled device camera (GIF 794, Gatan, Pleasanton, CA). To perform dual-axis transmission electron-microscopic tomography, Serial EM software[34] was employed to capture one image per degree of sample rotation (136 degrees in total). Tomographic reconstruction was performed by weighted back-projection with the IMOD software package; this yielded a contiguous stack of two-dimensional photomicrographs with ~4 nm resolution. The same software was used to trace subcellular structures on each section of the contiguous stack. We then compiled the traces to produce a 3-D rendition of the microdomain structure.

Immunogold Labeling

Whole animals were fixed similarly to immunohistochemical analysis. Brains were then removed and post-fixed in 4% paraformaldehyde (22 °C, 1 h) and cerebral arteries were isolated. In accordance with the Aurion immunogold reagent kit, fixed arteries were exposed to 0.1% sodium borohydride in PBS (15 min), 0.05% Triton X-100 (30 min), blocking solution 1 h at 4 °C and then PBS (2x10 min). Primary antibodies (1:100 dilution) were subsequently added to the buffer and incubated for 48 h at 4 °C. Tissues were subsequently washed with buffer (6x10 min), exposed to incubation medium containing ultra-small gold particles (0.8 nm labeled goat anti rabbit, 1:100 dilution, 48 h at 4 °C) and then washed with incubation buffer (6x10 min) and PBS (2x10 min). Prepared arteries were fixed again in PBS containing 2.5% glutaraldehyde (2 h) and then washed in PBS (2x10 min). Arteries were sequentially processed as follows: 1) enhancement conditioning solution (ECS, 4x10 min); 2) Silver enhancement solution (2 h); 3) 0.03 M sodium thiosulphate in ECS (10 min); 4) ECS wash (4x10 min); and 5) PBS wash (2x10 min). Tissues were then post-fixed for 1 h in a 1% osmium tetroxide-PBS solution, dehydrated in ethanol, and embedded in Epon resin. Ultrathin sections of about ~70 nm were cut, lightly stained with 2% aqueous uranyl acetate and Reynold's lead citrate (15 min), and viewed/photographed using a Hitachi H7650 transmission electron microscope (80 keV) and an AMT 16000 digital camera.

Immunohistochemistry

Rats were anaesthetized with sodium pentobarbital and perfused intra-cardially with 250 ml of PBS (pH 7.4), followed by 100 ml of 4% paraformaldehyde (pH 7.4) in PBS at room temperature. Brains were then removed and post-fixed in 4% paraformaldehyde for 1 h (22 °C). Posterior and middle cerebral arteries were subsequently excised and placed in a conical vial with standard working PBS solution containing 3% donkey, horse or goat serum, 0.1% Tween, and 1% dimethylsulphoxide (DMSO). Primary antibodies against smooth muscle actin (1:25 dilution), $Ca_V1.2$ (1:25 dilution), $Ca_V3.1$ (1:100 dilution), $Ca_V3.2$ (1:100 dilution), and RyR (1:100 dilution) were added to the working solution and incubated for 48 h (4 °C). Next, tissues were washed 3 times with PBS (15 min each, 22 °C) and incubated with working PBS solutions containing secondary antibodies (4 hr, 22 °C). Following washes with PBS, sections were mounted on gel-coated slides and covered with anti-fade medium, covered slips were sealed with nail polish and stored (-20 °C). Controls were obtained by omitting the 1ry antibodies or pre-adsorbing excess purified peptide. All reactions involved the use of fluorophore-conjugated secondary antibodies (1:1000 dilution): Alexa Fluor 488-donkey anti-mouse IgG, and Alexa

Fluor 555-goat anti-rabbit IgG. Immunolabelling was assessed using an Olympus FV300 BX50 confocal microscope equipped with Cy3 (555 nm, red) and FITC (488 nm, green) filter sets.

Proximity Ligation Assay (PLA)

The Duolink *in situ* PLA detection kit was employed using freshly isolated smooth muscle cells. Briefly, cells were fixed in PBS containing 4% paraformaldhyde (15 min), permeabilized in PBS containing 0.1% Tween (15 min), and quenched in PBS containing 100 mM glycine (5 min). Cells were then washed with PBS, blocked in Duolink blocking solution (30 min, 37 °C), and incubated overnight (4 °C) with primary antibodies (rabbit anti-$Ca_V3.2$ and mouse RyR_2) in Duolink antibody diluent solution. Control experiments employed no primary antibody or only one primary antibody. Cells were labelled with Duolink PLA PLUS and MINUS probes for 2 h (37 °C). The secondary antibodies of PLA PLUS and MINUS probes are attached to synthetic oligonucleotides that hybridize when in close proximity (<40 nm). The hybridized oligonucleotides are then ligated prior to rolling circle amplification. The amplification products extending from the oligonucleotide arm of the PLA probes were detected using red fluorescent fluorophore-tagged, complementary oligonucleotide sequences and a Zeiss Apotome epifluorescence microscope.

Computational Modeling

We have constructed a mathematical model that incorporates crucial ultrastructure and calcium handling features of the vascular smooth muscle cell in cerebral arteries. The smooth muscle cell is described as a cylinder, 76.5 μm in length and 5 μm in diameter, as shown in Fig. 5. For simulation purposes, a cell was subdivided into segments with each 8.5 μm in length. Based on microscopic data, in each segment there is a circumferential band, which is interrupted in approximately two locations, thus forming two discrete sections circumferentially. In the model, each segment is therefore further sub-divided into two semi-cylindrical “slices”. Simulations presented in this paper are based on the behavior of one slice. The frequency of Ca^{2+} spark-like events have been scaled to represent the whole cell, assuming that individual slices act independently. The model includes only mechanisms responsible for dynamic Ca^{2+} handling in the smooth muscle cell. This includes the sodium-calcium exchanger (NCX), plasma membrane Ca^{2+} ATPase (PMCA), sarco/endoplasmic reticulum Ca^{2+} ATPase (SERCA), ryanodine receptor (RyR), calmodulin, calsequestrin, and the Ca^{2+} channels $Ca_V1.2$, $Ca_V3.1$ and $Ca_V3.2$. In its present form, the model is limited to Ca^{2+} dynamics evoked by voltage-clamp stimuli. As illustrated in Fig. 5, the model explicitly accounts for an interaction between $Ca_V3.2$ and RyR in a restricted microdomain (subspace), representing the ~15 nm space between caveolae in the plasma membrane and the sarcoplasmic reticulum. Mathematically, the model comprises 12 ordinary differential equations, which were solved using the “ode15s” ODE solver in MATLAB (The MathWorks, Natick, MA, USA). See Supplemental appendix for a complete description of the model’s formulation.

Ca^{2+} Spark Measurements

Ca^{2+} sparks were measured in rat myocytes *in situ* using the en-face preparation technique[38] with the Ca^{2+} sensitive dye Fluo-4 AM using a Zeiss LSM 710 NLO laser scanning confocal imaging workstation on an inverted microscope platform (Zeiss Axio Observer Z1). Fluo-4 AM was dissolved in DMSO and added from a 1 mM stock to the arterial suspension at a final concentration of 10 μM, along with 0.1% pluronic F127 for 1-1.5 h at room temperature in

the dark in balanced salt solution. Arterial segments were then washed (30 min) to allow dye esterification and then cut into linear strips. The arterial segments were pinned to Sylgard blocks and placed in an open bath imaging chamber mounted on the confocal imaging stage. Cells were illuminated at 488 nm with a krypton argon laser and the emitted light was collected using a photomultiplier tube. Line scans were imaged at 529 fps with the emission signal recorded at 493-622. The acquisition period for Ca^{2+} spark recordings was 18.9 s. The resultant pixel size ranged from 0.068 to 0.11 μm per pixel. To ensure that sparks within the cell were imaged, the pinhole was adjusted to provide an imaging depth of 2.5 μm. This depth is roughly equivalent to the width of 50% of the cell based on morphological examination of live preparations, and was equivalent to our previous studies (data not shown). We performed analysis to characterize the percentage of cells with Ca^{2+} sparks and the frequency of firing. Sparks per 100 μm per second and the percentage of cells firing were computed from these observed sparks. Spatial and temporal characteristics of the Ca^{2+} spark events were calculated using the SparkMaster plug-in for ImageJ. These characteristics included: fractional fluorescence intensity; full duration at half maximum; full width at half maximum; and time to peak. The threshold for spark detection was 3.2 times the standard deviation of the background noise above the mean background level. Prior to analysis the background fluorescence was subtracted from each image assuming homogeneous background levels in each cell.

PCR Analysis

Smooth muscle cells (~200) isolated from cerebral arteries were placed in RNase- and DNase-free collection tubes. Total RNA was isolated from human cerebral artery smooth muscle cells using the RNeasy mini kit (Qiagen) whereas total RNA from human brain was purchased from Clontech. The RNA was reverse-transcribed using the Quantitect reverse transcription kit (Qiagen) according to manufacturer's instructions. A total of 1 ng cDNA was used to PCR amplify a 98 bp amplicon corresponding to $Ca_V3.2$ using the primer sequences $Ca_V3.2$-F (TGATTACCAGCATGCTCACG) and $Ca_V3.2$-R (GGTCTTCTTCTGCCTCGGTC) with Q5 DNA ploymerase (New England Biolabs) according to manufacturer's instructions. The PCR reactions were electrophoresed on a 1% agarose-TAE gel. Lane 1 is the PCR marker, lane 2 is the $Ca_V3.2$ amplicon from brain and lane 3 is the $Ca_V3.2$ amplicon from isolated smooth muscle cells.

Statistical Analysis

Data are expressed as means ± S.E., and n indicates the number of vessels or cells. No more than two different experiments were performed on vessels from a given animal. Where appropriate, paired, unpaired t-tests, or one way ANOVA were performed to compare the effects of a given condition/treatment on arterial diameter, or whole-cell current (see figure legends for specific details). *P values ≤ 0.05 were considered statistically significant.

Solutions and Chemicals

All buffers, chemicals and reagents originated from Sigma-Aldrich unless otherwise stated. Donkey and goat serum was purchased from Jackson Immuno-Research. Primary antibodies against smooth muscle actin were obtained from Abcam Inc. whereas those directed against $Ca_V1.2$, $Ca_V3.1$, $Ca_V3.2$, and RyR were purchased from Alomone. Secondary antibodies, which included Alexa Fluor 488-goat anti-mouse IgG and Alexa Fluor 555-goat anti-

rabbit IgG, were obtained from Invitrogen life Technologies. Aurion immunogold reagent and the PLA detection kit were purchased from Electron Microscopy Sciences and Olink, respectively.

Online Figure I

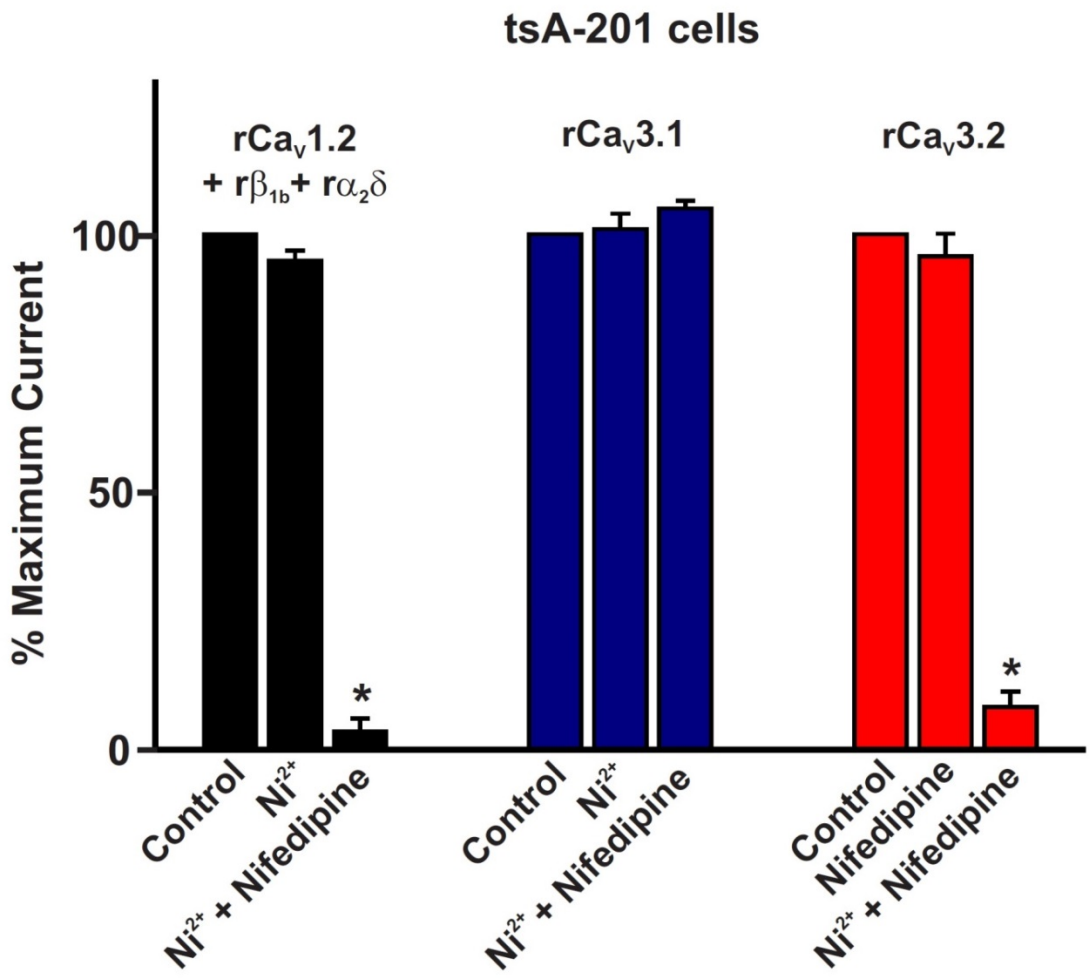

Online Figure I. Effects of Ni^{2+} and nifedipine on $Ca_V1.2$, $Ca_V3.1$ and $Ca_V3.2$ currents. Summary data of inward currents in tSA-201 cells transfected with $rCa_V1.2$, $rCa_V3.1$ or $rCa_V3.2$-cDNA. Experiments were performed in the absence and presence of Ni^{2+} (50 μM) or Nifedipine (200 nM). A voltage step from -90 to 0 mV was used to evoke inward Ba^{2+} current (n=5 each, * $P<0.05$, paired *t*-test). Ni^{2+} and nifedipine selectively block $Ca_V1.2$ and $Ca_V3.2$, respectively.

Online Figure II

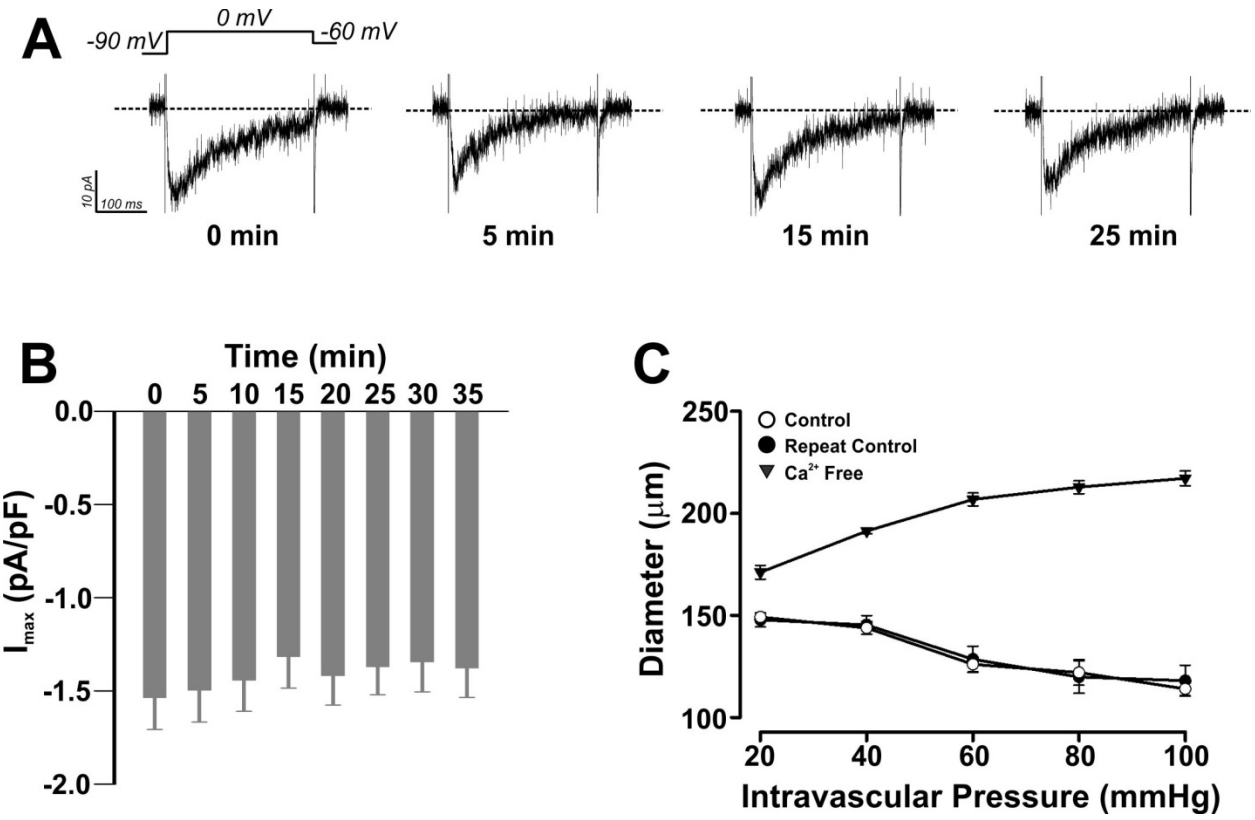

Online Figure II. Time control experiments. (A,B) Representative traces and summary data of T-type current in rat cerebral arterial smooth muscle cells over time (n=8). Experiments were performed in the presence of nifedipine (200 nM) to block L-type Ca^{2+} channels. A voltage step from -90 to 0 mV was used to elicit inward current. **(C)** Rat middle or posterior cerebral arteries were pressurized from 20 to 100 mmHg twice under control conditions; passive responses were ascertained in Ca^{2+}-free media (n=7). Electrical and vasomotor measurements were stable and repeatable over time.

Online Figure III

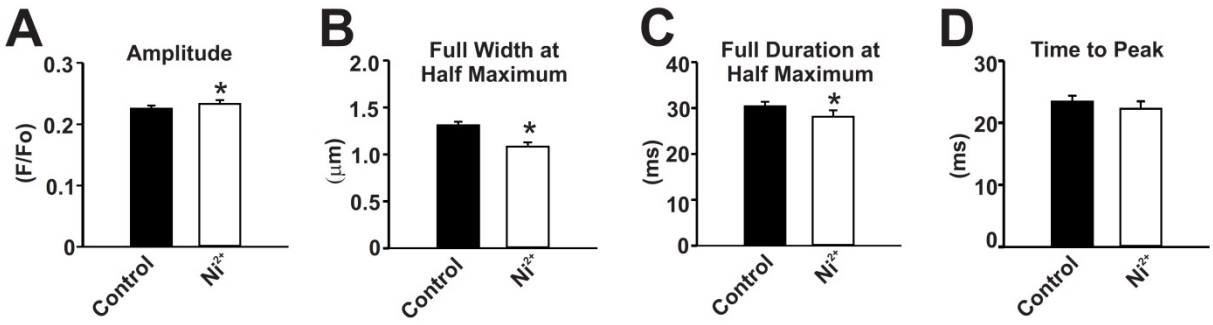

Online Figure III. Effects of Ni^{2+} on the kinetic characteristics of Ca^{2+} sparks. Line scan imaging performed on posterior and middle rat cerebral arteries to ascertain Ca^{2+} spark generation under control conditions and in the presence of Ni^{2+} (50 μM). Summary data characterizes the influence of Ni^{2+} on spatial (**A & B**) and temporal **(C & D**) characteristics of Ca^{2+} sparks (n=6 arteries, 291 line scans in total, **P*<0.05, paired *t*-test). Ni^{2+} elicited a limited but significant effect on the spatial and temporal characteristics of Ca^{2+} sparks.

Online Figure IV

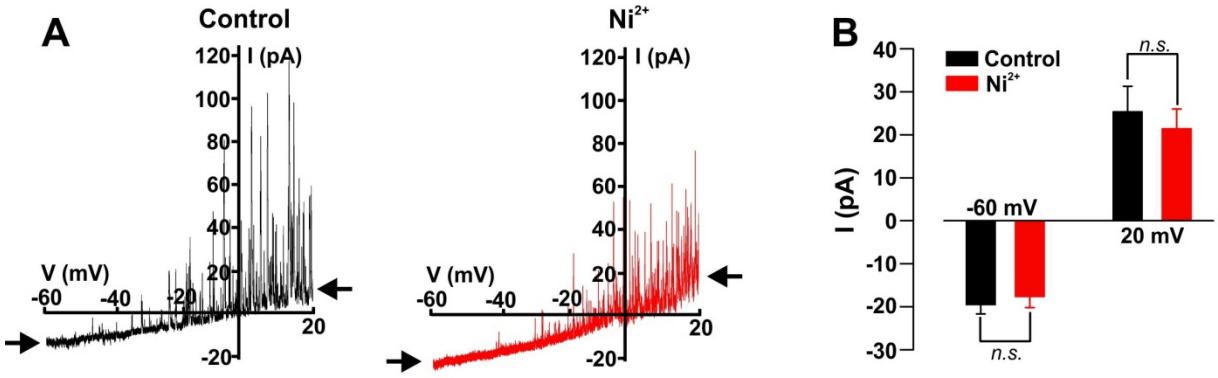

Online Figure IV. Ni^{2+} control experiments. (A,B) Representative traces and summary data of inward and outward current in rat cerebral arterial smooth muscle cells under control conditions and in the presence of Ni^{2+} (50 μM, n=10). Cells were slowly ramped from -60 to +20 mV (4 mV/s). Ni^{2+} had no effect on peak inward/outward current.

Supplemental Model Summary

1 Model and Method

Recent work has revealed a microdomain in cerebral arterial smooth muscle comprised of caveolae and sarcoplasmic reticulum. Immunolabeling techniques indicate that T-type Ca^{2+} channels and ryanodine receptors localize to this microdomain while L-type Ca^{2+} channels do not [3]. Given these observations, $Ca_v3.2$ channels were hypothesized to regulate a CICR response. To address this hypothesis, a mathematical model of a microdomain of rat cerebral vascular smooth muscle Ca^{2+} handling was developed. This model was based on parameters arising from tomographic, immunolabeling and electrical measurements of our lab and previous studies. It includes only the components responsible for Ca^{2+} dynamics in the SMC. In the following sections, the details of the model are explained.

2 Slice

A typical vascular smooth muscle cell from rat cerebral artery has a fusiform shape. In our model, we consider it as a cylinder with a length of about 80 µm and a diameter of 5 µm (Figure 1). A slice is considered to be the volume of the cell that is devoid of actin and includes the peripheral SR, its adjacent caveolae and the space between them which is denoted the subspace. Based on microscopic data [3], in each ≈8.5 µm length of the cell, there is a circumferential band which includes 2 discrete slices. Therefore, each slice is a half cylinder of length of 8.5 µm as illustrated in Figure 1.

The model includes only the components responsible for Ca^{2+} dynamics in the SMC. This comprises the Sodium-Calcium Exchanger (NCX), Plasma membrane Ca^{2+} ATPase (PMCA), Sarcoplasmic reticulum, Sarco/endoplasmic reticulum Ca^{2+} ATPase (SERCA), Ryanodine receptor, Calmodulin, Calsequestrin, ans the calcium channels $Ca_v1.2$, $Ca_v3.1$ and $Ca_v3.2$. The model is based on a set of 11 ordinary differential equations (Equations 1, 3, 6, 8, 13, 18, 24, 27, 32, 33 and 34).

3 Myoplasmic Calcium

The subspace (the dark blue area in Figure 1 immediately under the cell membrane) has a depth of 10 to 15 nm [3]. Two channels inject their currents into the subspace: T-type Ca^{2+} ($I_{Ca_v3.2}$), and RyR (J_{rel}). The Ca^{2+} concentration within the subspace, denoted $[Ca^{2+}]_{SS}$, diffuses into the cytosol (J_{xfer}). The buffer calmodulin (CMDN) was also assumed present in the subspace:

$$\frac{d[Ca^{2+}]_{SS}}{dt} = B_{SS}\left(J_{rel}\frac{V_{JSR}}{V_{SS}} - J_{xfer}\frac{V_{myo}}{V_{SS}} + I_{Ca_v3.2}\frac{A_{cap}C_m}{2V_{SS}F}\right) \tag{1}$$

$$B_{SS} = \left\{1 + \frac{[CMDN]_{tot}K_m^{CMDN}}{(K_m^{CMDN} + [Ca^{2+}]_{SS})^2}\right\}^{-1} \tag{2}$$

Calcium in the cytosol, $[Ca^{2+}]_i$, is further influenced by leak from the sarcoplasmic reticulum (J_{leak}), uptake by the SERCA pump (J_{up}), extrusion by the PMCA pump (I_{PCMA}), L-type Ca^{2+} channels (I_{CaL}), the sodium calcium exchanger (I_{NCX}), T-type Ca channels ($I_{ca_v3.1}$) and a background Ca^{2+} channel ($I_{Ca,b}$). Again, calmodulin was present:

$$\frac{d[Ca^{2+}]_i}{dt} = B_i\left(J_{leak} + J_{xfer} - J_{up} - \left(I_{Ca,b} + I_{PMCA} + I_{Ca,L} + I_{Ca_v3.1} - 2I_{NCX}\right)\frac{A_{cap}C_m}{2V_{myo}F}\right) \tag{3}$$

$$B_i = \left\{1 + \frac{[CMDN]_{tot}K_m^{CMDN}}{(K_m^{CMDN} + [Ca^{2+}]_i)^2}\right\}^{-1} \tag{4}$$

$$J_{xfer} = \frac{[Ca^{2+}]_{SS} - [Ca^{2+}]_i}{\tau_{xfer}} \tag{5}$$

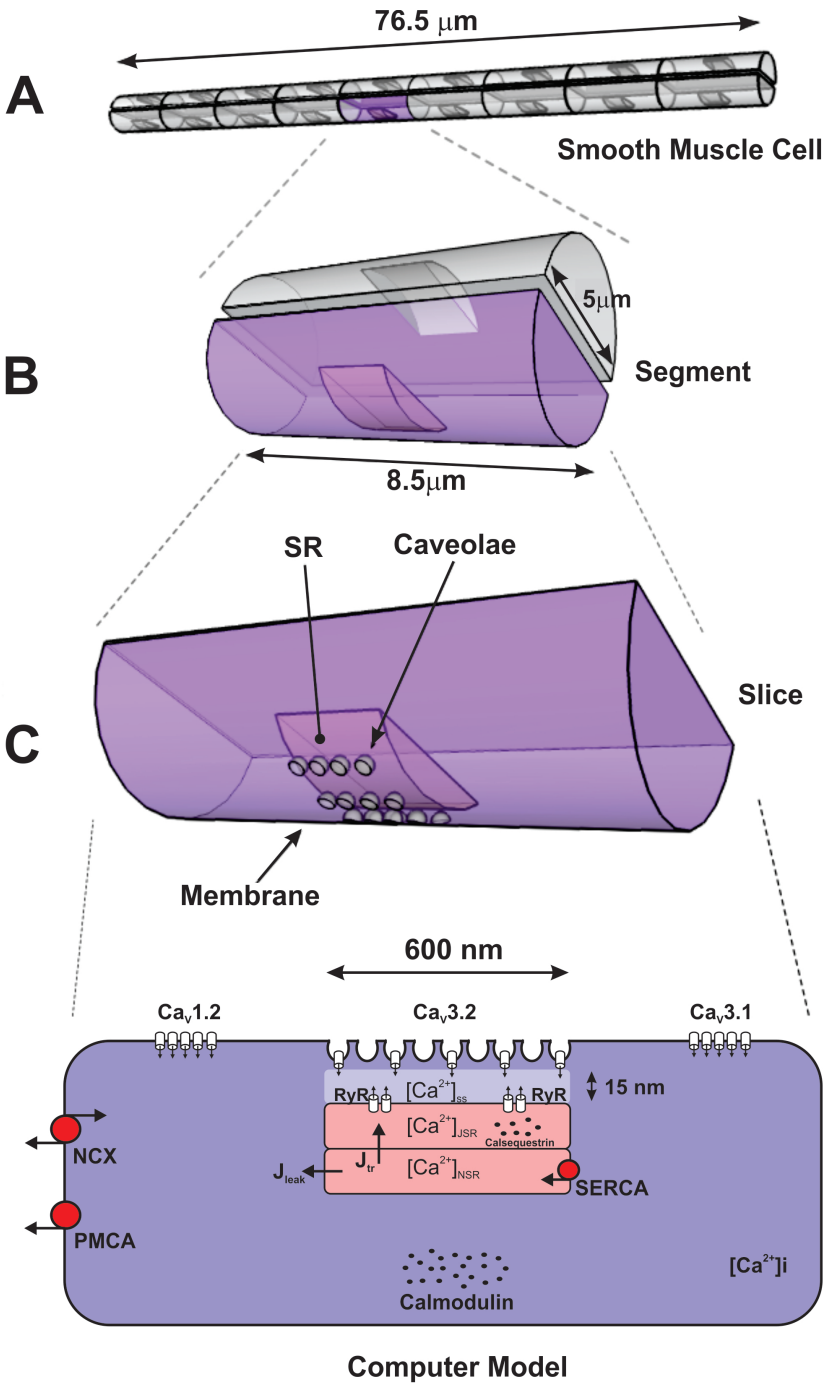

Modeling Figure 1: **Top**: One smooth muscle cell (A) is divided into cylindrical segments (B) which are composed of two slices(C). **Bottom**: Schematic representation of a slice. The slice includes Sodium-Calcium Exchanger (NCX), Plasma membrane Ca^{2+} ATPase (PMCA), the Sarcoplasmic Reticulum which has two parts: Uptake (lower pink) and Release (upper pink), Sarco/Endoplasmic Reticulum Ca^{2+} ATPase (SERCA), Ryanodine Receptor (RyR), Buffers: Calmodulin, Calsequestrin, and Ca^{2+} Channels: $Ca_v1.2$, $Ca_v3.1$ and $Ca_v3.2$

Myoplasmic Calcium parameters			
Parameter	**Definition**	**Value**	**Unit**
V_{myo}	Volume of the cytoplasm	6.5450e-08	μL
V_{JSR}	Junctional SR volume	3.2725e-10	μL
V_{NSR}	Network SR volume	6.54509e-10	μL
V_{ss}	Subspace volume	8.325e-11	μL
C_m	membrane capacitance	1.0	$\mu F/cm^2$
A_{cap}	Capacitive membrane area	5.2360e-07	cm^2
F	Faraday's constant	96.5	Col /mol
$[CMDN]_{total}$	Total myoplasmic calmodulin concentration	50	μM
K_m^{CMDN}	half-saturation constant for calmodulin	0.238	μM
τ_{xfer}	Time constant for transfer from subspace to cytoplasm	6.96	ms

4 Sarcoplasmic Reticulum

The model of sarcoplasmic reticulum consists of two parts: uptake (also called the network sarcoplasmic reticulum, NSR) and release (also called the junctional sarcoplasmic reticulum, JSR). The uptake part contains the SERCA pump. Moreover, Ca^{2+} passive release, also called Ca^{2+} leak, is modeled to take place in the uptake portion. The release compartment contains the Ca^{2+} buffer calsequestrin (CSQN) and RyR channels. The Ca^{2+} flux between these two subcompartments is designated by J_{tr}.

Ca^{2+} uptake into the SR (J_{up}) was described by the Hill equation (Eq. 11). The value of SR Ca2-ATPase maximum pump rate and half-saturation constant have been adjusted. The mathematical relations describing the sarcoplasmic reticulum are derived from [2]:

$$\frac{d[Ca^{2+}]_{JSR}}{dt} = B_{JSR}(J_{tr} - J_{rel}) \tag{6}$$

$$B_{JSR} = \left\{1 + \frac{[CSQN]_{tot} K_m^{CSQN}}{(K_m^{CSQN} + [Ca^{2+}]_{JSR})^2}\right\}^{-1} \tag{7}$$

$$\frac{d[Ca^{2+}]_{NSR}}{dt} = (J_{up} - J_{leak})\frac{V_{myo}}{V_{NSR}} - J_{tr}\frac{V_{JSR}}{V_{NSR}} \tag{8}$$

$$J_{leak} = \nu_{leak}([Ca^{2+}]_{NSR} - [Ca^{2+}]_i) \tag{9}$$

$$J_{tr} = \frac{[Ca^{2+}]_{NSR} - [Ca^{2+}]_{JSR}}{\tau_{tr}} \tag{10}$$

$$J_{up} = \nu_{up}\frac{[Ca^{2+}]_i^2}{K_{m,up}^2 + [Ca^{2+}]_i^2} \tag{11}$$

SR Parameters			
Parameter	**Definition**	**Value**	**Unit**
ν_{leak}	maximum Ca^{2+} leak rate from the NSR to cytosol	2.5463e-05	ms^{-1}
ν_{up}	maximum uptake rate of SERCA pump	0.5352	$\mu M/ms$

τ_{tr}	Time constant for transfer from NSR to JSR	20	ms
$[CSQN]_{total}$	Total junctional SR calsequestrin concentration	15000	μM
K_m^{CSQN}	Ca^{2+} half-saturation constant for calsequestrin	800	μM
$K_{m,up}$	Half-saturation constant of SERCA pump	0.7766	μM

5 T-type Ca^{2+} Channels

Two isoforms of the T-type Ca^{2+} channel exist in vascular smooth muscle cell: $Ca_v3.1$ and $Ca_v3.2$ [3]. Based on Immunolabeling data [3], the former has a diffusive distribution throughout the membrane. In contrast, $Ca_v3.2$ is mainly expressed in the caveolae. They are found mostly in clusters directly opposed to ryanodine receptors on the sarcoplasmic reticulum [3]. We hypothesized that Ca^{2+} which enters the cell as $I_{Cav3.2}$ results in a localized increase in $[Ca^{2+}]_{ss}$. We put the $Ca_v3.1$ splice variant along the cell and $Ca_v3.2$ were localized only in the caveolae. We have adopted the T-type Ca^{2+} channel mathematical model from Purkinje fibers in rabbit heart [1] for both isoforms.

The equations describing the channel are given below with b and g being gating variables. For channel X, x_∞ is the steady state value, τ_X is the time constant, α_X is the transition rate from non-permissive to permissive state, and β_X is rate of the opposite transition.

$$I_{Ca_v3.X} = g_{Ca_v3.X}\, b\, g\, (V - E_{CaT}) \tag{12}$$

$$\frac{db}{dt} = \frac{b_\infty - b}{\tau_b} \tag{13}$$

$$b_\infty = \frac{1}{1 + e^{(v+28)/6.1}} \tag{14}$$

$$\tau_b = \frac{1}{\alpha_b + \beta_b} \tag{15}$$

$$\alpha_b = 1.068e^{(v+16.3)/30} \tag{16}$$

$$\beta_b = 1.068e^{-(v+16.3)/30} \tag{17}$$

$$\frac{dg}{dg} = \frac{g_\infty - g}{\tau_g} \tag{18}$$

$$g_\infty = \frac{1}{1 + e^{(v+60)/6.6}} \tag{19}$$

$$\tau_g = \frac{1}{\alpha_g + \beta_g} \tag{20}$$

$$\alpha_g = 0.015e^{-(v+71.7)/83.33} \tag{21}$$

$$\beta_g = 0.015e^{-(v+71.7)/15.38} \tag{22}$$

T-type Channel parameters			
Parameter	**Definiton**	**Value**	**Units**
$g_{Ca_v3.1}$	maximum $Ca_v3.1$ conductance	0.0684	mS/cm^2
$g_{Ca_v3.2}$	maximum $Ca_v3.2$ conductance	0.1026	mS/cm^2
E_{CaT}	Reversal potential	50	mV

6 L-type Ca^{2+} Channel

L-type Ca^{2+} channels ($Ca_v1.2$) are spread along the long axis of the smooth muscle cell [3] and have a distinct distribution in comparison with $Ca_v3.2$ channels which run perpendicular to the long axis of SMC.

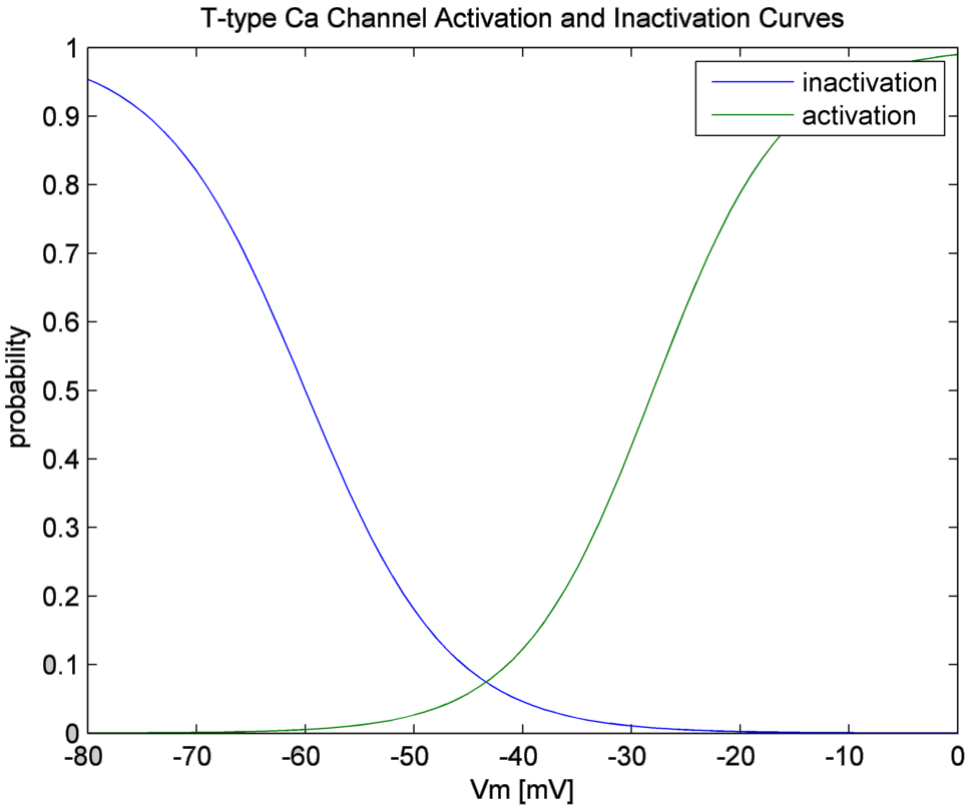

Modeling Figure 2: T-type Ca^{2+} channel (both $Ca_v3.1$ and $Ca_v3.2$) activation and inactivation curves

Thus, we have placed L-type Ca^{2+} channel throughout the slice but out of the caveolae as there is no spatial correlation between them and the caveolae.

Innate smooth muscle L-type $Ca_v1.2$ calcium channels have been shown to contain a fraction of Ca^{2+} currents with a window current that is close to resting potential[8]. The voltage-dependence of the activation curve of smooth muscle L-type Ca^{2+} channels shows a hyperpolarized shift of -15 mV in comparison with those of cardiac cells [7]. If the voltage-dependence of L-type Ca^{2+} channels of smooth muscle cells were similar to that of cardiac cells, only a small amount of contraction would be generated by smooth muscle cells[7]. Therefore, we modified an L-type model of rabbit cardiac cells [1] by shifting the activation to the left by 15 mV (Figure 3) and scaling the conductance, g_{CaL}, according to the experimental data obtained from rat cerebral arteries in our lab [3]. Equations for the channel are given below with d and f being the gating variables:

$$I_{CaL} = g_{CaL}(1 - f_{Ca})\, d\, f\, (V - E_{CaL}) \tag{23}$$

$$\frac{dd}{dt} = \frac{d_\infty - d}{\tau_d} \tag{24}$$

$$d_\infty = \frac{1}{1 + e^{-(v+11)/6.74}} \tag{25}$$

$$\tau_d = \frac{0.59 + 0.8e^{0.52(v+28)}}{1 + e^{0.132(v+28)}} \tag{26}$$

$$\frac{df}{dt} = \frac{f_\infty - f}{\tau_f} \tag{27}$$

$$f_\infty = \frac{1}{1 + e^{(v+40)/10}} \tag{28}$$

$$\tau_f = 0.005(v + 12.5)^2 + 4 \tag{29}$$

L-type Channel parameters			
Parameter	**Definiton**	**Value**	**Units**
g_{CaL}	maximum conductance	0.0641	mS/cm^2
E_{CaL}	Reversal potential	63	mV

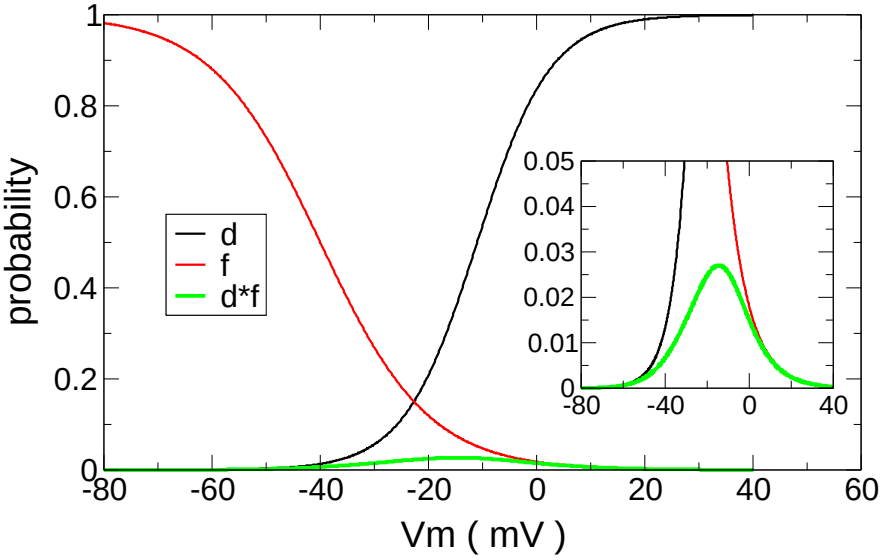

Modeling Figure 3: L-type Ca^{2+} Channel Activation and Inactivation Curves. f and d are the inactivation and activation parameters. The inset zooms in on the product of d and f.

There is another important difference between smooth muscle L-type $Ca_v1.2$ Ca^{2+} channels and those of the cardiac tissue. Data obtained in our lab show that the smooth muscle splice does not exhibit Ca^{2+}-dependent inactivation in steady-state current (Figure 4). It is known that Ba^{2+} does not cause Ca^{2+}-dependent inactivation because it does not affect the channel chemically to inactivate it. Thus, if the Ba^{2+} and Ca^{2+} traces are the same for the channel, it means the channel does not go through Ca^{2+}-dependent inactivation. Figure 4 shows the percentage of the channels which are in the inactivation state for Ba^{2+} and Ca^{2+} at different times. At 1500 ms, there is no difference between the Ba^{2+} and Ca^{2+} traces, indicating that the steady-state Ca^{2+}-dependent inactivation does not exist for smooth muscle L-type $Ca_v1.2$ Ca^{2+} channels.

7 Background Calcium Current

The background calcium current was modelled as a simple ohmic leak:

$$I_{Ca,b} = g_{Ca,b}(V - E_{CaL}) \tag{30}$$

Background Ca^{2+} Channel parameters			
Parameter	**Definition**	**Value**	**Unit**
g_{CaB}	Maximum conductance	3.670e-05	$\mu S/cm^2$

8 Ryanodine Receptor Channel

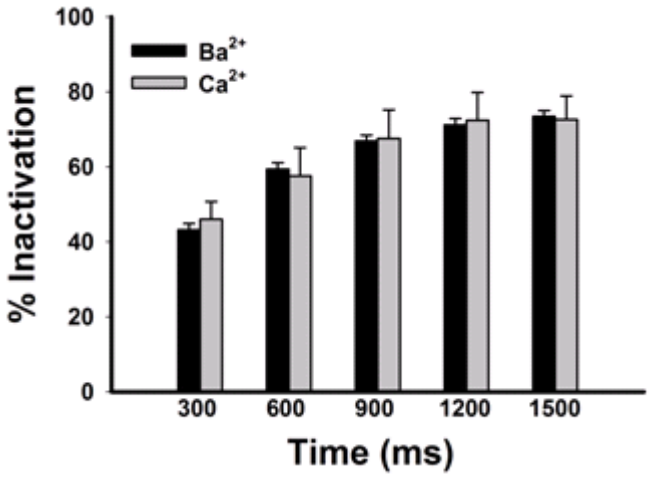

Modeling Figure 4: Some smooth muscle splice variants show minimal Ca^{2+}-dependent steady state inactivation

The model of Keizer, J *et al.*[5] with some modifications in their rates has been adopted. The modifications were determined using parallel multi-objective genetic algorithm [4] in order to reproduce experimental data. More specifically, the object functions were set to produce repetitive CICR responses with an appropriate period, $[Ca^{2+}]_{ss}$ amplitude, average $[Ca^{2+}]_i$ amplitude and basal $[Ca^{2+}]_i$ level.

This RyR model consists of two close and two open states. See Figure 5. State C_1 and C_2 are closed states while O_1 and O_2 are open states. These states are considered to be states of the entire RyR rather than states of the four subunits. A channel is in one of the states, X, with probability P_X. Transition from C_1 to O_1 and from O_1 to O_2 were considered to be Ca^{2+} dependent. The second open state, O_2 has the important role of increasing the open probability during the plateau as $[Ca^{2+}]_{ss}$ is elevated . The plateau open probability is shown in Figure 7.

Figure 6 shows RyR open probability when $[Ca^{2+}]_{ss}$ is stepped from 0.1 uM to 5 uM. The initial increase to peak happens on the millisecond time scale, whereas the decline to the plateau level occurs over several hundreds of milliseconds. The extent of opening immediately after Ca^{2+} stimulation (the peak open probability) and that after inactivation (the plateau) both increase with increasing $[Ca^{2+}]_{ss}$. Figure 7 illustrates the peak and the plateau (steady-state value) open probabilities at different $[Ca^{2+}]_{ss}$levels. At lower concentrations, the open probability rises quickly and then decreases to the plateau slowly. However, at higher $[Ca^{2+}]_{ss}$, after reaching the peak, RyR stays open and inactivation is negligible.

$$J_{rel} = \nu(P_{O1} + P_{O2})([Ca^{2+}]_{JSR} - [Ca^{2+}]_{SS}) \tag{31}$$

$$\frac{dP_{C1}}{dt} = k_a^- P_{O1} - k_a^+ [Ca^{2+}]_{SS}^n P_{C1} \tag{32}$$

$$\frac{dP_{O2}}{dt} = k_b^+ [Ca^{2+}]_{SS}^m P_{O1} - k_b^- P_{O2} \tag{33}$$

$$\frac{dP_{C2}}{dt} = k_c^+ P_{O1} - k_c^- P_{C2} \tag{34}$$

$$P_{O1} = 1 - (P_{C1} + P_{C2} + P_{O2}) \tag{35}$$

RyR Channel parameters			
Parameter	**Definition**	**Value**	**Unit**
ν	Maximum permeability	4.5	ms^{-1}

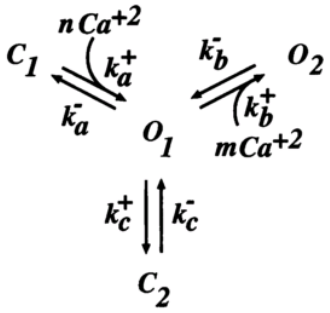

Modeling Figure 5: Schematic diagram of transition among the four states of RyR channel. C_1 and C_2 are closed states whereas O_1 and O_2 are open states. Transition from C_1 to O_1 and also transition from O_1 to O_2 are Ca^{2+} dependent.

k_a^+	$P_{C1} - P_{O1}$ rate	0.02050	$\mu M^{-n} ms^{-1}$
k_a^-	P_{O1} - P_{C1} rate	0.05205	ms^{-1}
k_b^+	$P_{O1} - P_{O2}$ rate	0.0094	$\mu M^{-m} ms^{-1}$
k_b^-	$P_{O2} - P_{O1}$ rate	0.1920	ms^{-1}
k_c^+	$P_{O1} - P_{C2}$ rate	0.0778	ms^{-1}
k_c^-	$P_{C2} - P_{O1}$ rate	0.0035	ms^{-1}
m	$P_{O1} - P_{O2}$ cooperativity	3	dimensionless
n	$P_{C1} - P_{O1}$ cooperativity	4	dimensionless

This RyR model consists of two close and two open states. State C_1 and C_2 are closed states. States O_1 and O_2 are open states. These states are considered to be states of the entire RyR rather than states of the four subunits. As it is illustrated in Figure 5, transition from C_1 to O_1 and from O_1 to O_2 are considered to be Ca^{2+} dependent. The second open state, O_2 has an important role of keeping the plateau open probability increasing as $[Ca^{2+}]_{ss}$ is elevated [5]. The plateau open probability is shown in Figure 7.

Figure 6 shows the RyR open probability when $[Ca^{2+}]_{ss}$ is elevated from 0.1 µM to 5 µM . The initial increase to peak happens on the millisecond time scale, whereas the decline to the plateau occurs within several hundreds of milliseconds. The extent of opening immediately after Ca^{2+} stimulation (the peak open probability) and that after inactivation (the plateau) both increase with increasing $[Ca^{2+}]_{ss}$. Figure 7 illustrate the peak and the plateau (steady-state value) of open probability at different $[Ca^{2+}]_{ss}$ level. At lower concentrations, the open probability rises quickly and then decreases to the plateau slowly. However as the figures indicates, at higher $[Ca^{2+}]_{ss}$, after reaching the peak, RyR stays open and inactivation is negligible. This shows that RyR inactivation is Ca^{2+}-dependent in the model.

9 Ca^{2+} Extrusion Mechanisms

The model of NCX and PMCA were adopted from Bondarenko *et al.* [2] and the exchanger scaling factor (k_{NaCa}) was adjusted (by using GA) so that the basal level of $[Ca^{2+}]_i$ agreed with physiological values.

$$I_{NCX} = k_{NaCa} \frac{1}{k_{mNa}^3 + [Na^+]_o^3} \frac{1}{k_{mCa} + [Ca^{2+}]_o} \frac{1}{1 + \kappa_{sat}^{(\eta-1)VF/RT}} \times \left\{ e^{\eta VF/RT} [Na^+]_i^3 [Ca^{2+}]_o - e^{(\eta-1)VF/RT} [Na^+]_o^3 [Ca^{2+}]_i \right\} \tag{36}$$

$$I_{PCMA} = I_{PCMA}^{max} \frac{[Ca^{2+}]_i^2}{K_{m,pCa}^2 + [Ca^{2+}]_i^2} \tag{37}$$

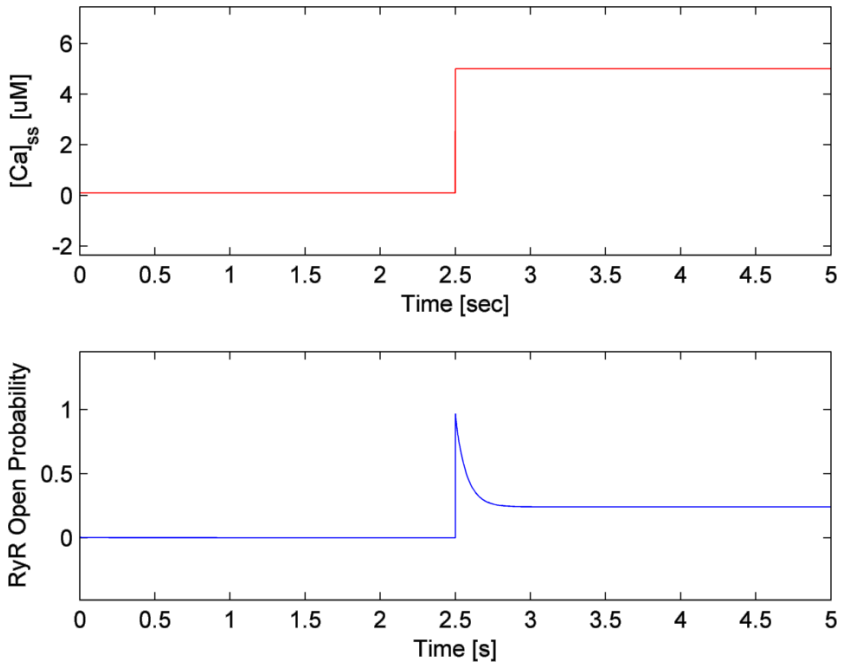

Modeling Figure 6: A simulation of the rapid rise to peak open probability of a single RyR following an increase of $[Ca^{2+}]_{ss}$ from 0.1 to 5 µM.

NCX parameters			
Parameter	**Definition**	**Value**	**Unit**
k_{NaCa}	scaling factor	1.464e+02	$\mu A/cm^2$
K_{mNa}	Na^+ half-saturation constant	87500	μM
K_{mCa}	Ca^{2+} half-saturation constant	1380	μM
K_{sat}	saturation factor for large negative potentials	0.1	dimensionless
η	voltage dependence	0.35	dimensionless
T	temperature	293.15	K
R	Ideal gas constant	8.314	$JK^{-1}mol^{-1}$
$[Ca^{2+}]_o$	Extracellular Ca^{2+} concentration	1800	μM
$[Na]_o$	Extracellular Na concentration	1.400e+04	μM
$[Na]_i$	Intracellular Na concentration	1.4237e+04	μM

PMCA parameters			
Parameter	**Definition**	**Value**	**Unit**
I_{PMCA}^{max}	max rate	1.2	$\mu A/cm^2$
$K_{m,pCa}$	Ca^{2+} half-saturation constant	0.500	μM

10 Initial Conditions

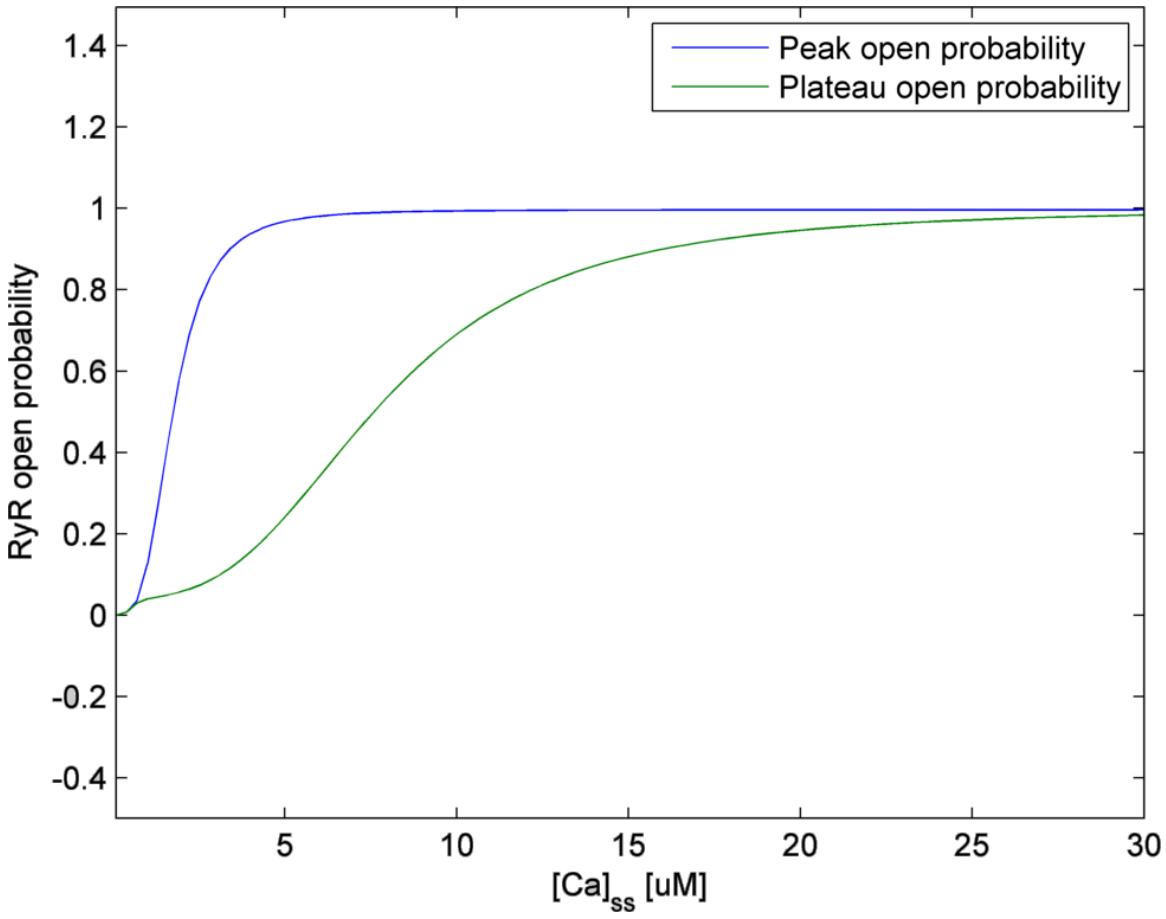

Modeling Figure 7: The peak and the plateau open probabilities increases with increasing $[Ca^{2+}]_{ss}$ indicating RyR inactivation is a Ca^{2+}-dependent process

Initial Conditions			
Parameter	**Definition**	**Value**	**Unit**
t	Time	0.0	ms
V	Membrane Potential	-60	mV
$[Ca^{2+}]_i$	Cytosolic Ca^{2+} concentration	0.1209	μM
$[Ca^{2+}]_{SS}$	Subspace Ca^{2+} concentration	0.1505	μM
$[Ca^{2+}]_{JSR}$	JSR Ca^{2+} concentration	0.300	μM
$[Ca^{2+}]_{NSR}$	NSR Ca^{2+} concentration	0.300	μM
P_{C1}	Fraction of channels in State P_{C1}	0.4298	dimensionless
P_{C2}	Fraction of channels in State P_{C2}	0.4298	dimensionless
P_{O1}	Fraction of channels in State P_{O1}	0.1404	dimensionless
P_{O2}	Fraction of channels in State P_{O2}	1.0030e-05	dimensionless

11 Numerical Methods

The model was implemented in MATLAB™ and 12 differential equations were solved with the ode15s routine for stiff systems [6]. We used multi-objective parallel genetic algorithm to adjust various parameters in the model in order to obtain experimentally-consistent results. To implement the optimization, the Parallel Computing toolbox and Global Optimization toolbox of MATLAB™ software package were used.

We chose this multi-objective optimization as there were several (and conflicting) objective functions. These objective functions rewards sets of parameters that cause the behaviors of model to be to be consistent with the experimental data including the following items:

- Frequency of oscillation ˜1 Hz
- Steady-state $[Ca^{2+}]_i$ of 100 nM
- Average $[Ca^{2+}]_i$ in the range 200-250 nM at -40 mV
- No oscillations at ˜-60 mV
- Sustained oscillations at a reduced frequency after $Ca_v1.2$ blockade

The optimization was used to modify the RyR transition rates (k_a^-,k_a^+, k_b^-, k_b^+,k_c^-,k_c^+), leakage current from SR into the cytosol (ν_{leak}), the NCX maximum rate (k_{NaCa}) and the diffusion rate from the subspace into the cytosol (τ_{xfer}). Changes in those parameters were mostly within 20% of the original values. The most appropriate solution was selected among the Pareto optima.

As the each run of simulation took 10s, for speeding up the GA convergence, we used a parallel multi-objective GA. This optimization algorithm was run on an Intel(R) 4-Core(TM) i7-2600K CPU @ 3.40GHz.

References

[1] Oleg V. Aslanidi, Rakan N. Sleiman, Mark R. Boyett, Jules C. Hancox, and Henggui Zhang. Ionic mechanisms for electrical heterogeneity between rabbit purkinje fiber and ventricular cells. *Biophys J*, 98(11):2420–2431, Jun 2010.

[2] Vladimir E. Bondarenko, Gyula P. Szigeti, Glenna C L. Bett, Song-Jung Kim, and Randall L. Rasmusson. Computer model of action potential of mouse ventricular myocytes. *Am J Physiol Heart Circ Physiol*, 287(3):H1378–H1403, Sep 2004.

[3] R. A. El-Rahman, S. E. B. Welsh, Y. Anfinogenova, O. Harraz, R. Turner, and D. G. Welsh. L- and t-type calcium channels in cerebral arteries. In *The FASEB Journal*, volume vol. 25, page 1024.18, 2011.

[4] D. E. Goldberg. *Genetic Algorithms in Search. Optimization, and machine Learning.* Addison-Wesley Longham Publishing Co, Inc, Boston, MA, USA, 1st edition, 1989.

[5] J. Keizer and L. Levine. Ryanodine receptor adaptation and ca2+(-)induced ca2+ release-dependent ca2+ oscillations. *Biophys J*, 71(6):3477–3487, Dec 1996.

[6] Mark W. Reichelt Lawrence F. Shampine. The Matlab ODE suite. *SIAM Journal Scientific Computing*, 18(1):1, 1997.

[7] Ping Liao, Tan Fong Yong, Mui Cheng Liang, David T. Yue, and Tuck Wah Soong. Splicing for alternative structures of cav1.2 ca2+ channels in cardiac and smooth muscles. *Cardiovasc Res*, 68(2):197–203, Nov 2005.

[8] Ping Liao, Dejie Yu, Guang Li, Tan Fong Yong, Jia Lin Soon, Yeow Leng Chua, and Tuck Wah Soong. A smooth muscle cav1.2 calcium channel splice variant underlies hyperpolarized window current and enhanced state-dependent inhibition by nifedipine. *J Biol Chem*, 282(48):35133–35142, Nov 2007.